DOI: 10.15825/1995-1191-2026-1-242-254

INFLUENCE OF LEAFLET CALCIFICATION PATTERNS ON THE BIOMECHANICS OF BIOPROSTHETIC MITRAL VALVES

P.S. Onishchenko, K.Yu. Klyshnikov, T.V. Glushkova, A.E. Kostyunin, O.L. Barbarash, E.A. Ovcharenko

Research Institute for Complex Issues of Cardiovascular Diseases, Kemerovo, Russian Federation

Objective: to identify characteristic patterns of calcium distribution in explanted bioprosthetic heart valves and evaluate their influence on the biomechanics of the device. **Materials and methods.** Thirty-three bioprosthetic mitral valve leaflets explanted due to structural valve degeneration were analyzed. Multislice computed tomography (MSCT) images were used to identify pathological calcification within each leaflet. Calcified regions were segmented from top-view projections using a radiographic density threshold of 130 HU. The resulting dataset was clustered according to the number of pixels representing calcified areas, yielding three distinct classes: no calcification, mild calcification, and severe calcification. For each class, a three-dimensional computational model of the bioprosthesis was constructed. Biomechanical behavior was evaluated numerically in a series of computer simulation experiments using the finite element method. Each model included the supporting frame and three valve leaflets, with physiologically relevant boundary conditions simulating pressures in the left atrium and left ventricle. The analysis assessed maximum principal stress, strain, and their spatial distribution across the prosthesis. **Results**. Calcification of one or two valve leaflets resulted in a slight reduction in the average stress and strain values of the intact leaflet – from 0.319 to 0.303 MPa and from 0.134 to 0.130 mm/mm, respectively. Increased calcium content also lowered the peak stress and strain values, from 2.884 to 2.117 MPa and from 0.384 to 0.333 mm/mm. A clear relationship was observed between calcification pattern and local stress concentrations, which exceeded the leaflet's mean stress values by 40–50%. Co-localization of mild or severe calcification clusters on one or two leaflets produced qualitative alterations in the closure mechanism, including "overlap" of mineralized leaflets over adjacent intact ones. **Conclusion.** The findings demonstrate a relationship between the stress–strain behavior of bioprosthetic valve leaflets and the spatial pattern of calcification. While an increase in calcium volume up to 28% does not substantially affect mean stress or strain values, it significantly reduces their peak values.

Keywords: mitral valve, bioprosthetic heart valve, calcification, MSCT segmentation, clustering, finite element method, biomechanics.

INTRODUCTION

In Russia, 2,526 bioprosthetic heart valves (BHVs) were surgically implanted in 2022 [1], with more than 1,600 procedures performed using minimally invasive techniques [2]. Unlike mechanical valves, BHVs do not require long-term anticoagulant therapy and provide hemodynamic performance comparable to that of native heart valves. However, according to reports, more than half of implanted BHVs require replacement within 10–15 years due to structural valve degeneration (SVD) [3]. The main cause of SVD is calcification of the valve apparatus [4, 5]. This process is characterized by progressive calcium deposition within prosthetic tissues, leading to reduced leaflet elasticity and impaired functional mobility.

However, despite extensive research on this issue, there remains no consensus on the root cause of BHV calcification. Several studies highlight the limited understanding of the processes involved [6]. Some authors attribute calcification to immune-mediated responses, including reactions to residual xenogeneic cells [7] or to fixation and stabilization treatments applied to bioprosthetic materials [8]. Sinusas [9] has emphasized that, in addition to valve design and hemodynamic factors, mechanical stresses play a critical role in the development of SVD.

Advances in analytical tools have expanded the investigation of SVD to include numerical modeling approaches, which provide insight into the stress–strain state of BHVs and their components [10–14]. For instance, Qin et al. (2020) investigated calcification using 3D, patient-specific models of six bicuspid aortic valves [14]. Using finite element method (FEM), the authors evaluated valve biomechanics while accounting for calcium deposits on leaflet surfaces and demonstrated a direct relationship between areas of high mechanical stress and calcification sites.

Similarly, Arzani et al. (2017) demonstrated the influence of leaflet stretching on both the direction and

Corresponding author: Pavel Onishchenko. Address: 6, Akademika Barbarasha bul'var, Kemerovo, 650002, Russian Federation. Phone: (3842) 34-55-86, ext. 6488. E-mail: onisps@kemcardio.ru

intensity of mineralization in a native aortic valve model [15]. Their findings suggested that calcification initiates at leaflet attachment sites and progresses centripetally, driven by stiffness mismatches between calcified regions and surrounding tissue.

Overall, the findings reported above do not allow for the formulation of a unified, albeit multifactorial, opinion about the root cause and mechanisms of calcification progression. Therefore, the present study aims to investigate the relationship between mineralization patterns and mechanical stress distribution using our own collection of explanted BHVs in the mitral position, combined with numerical biomechanical analysis.

MATERIALS AND METHODS

The study material consisted of UniLine prosthetic xenopericardial heart valves (NeoCor, Russia) explanted electively due to SVD. All procedures were conducted at the surgical department of the Research Institute for Complex Issues of Cardiovascular Diseases in Kemerovo. Between 2015 and 2024, a total of 11 mitral-position BHVs were included in the study, with no cases excluded. The duration of prosthesis function in the analyzed cohort had a median of 5.33 years (interquartile range: 0.96–9.62), with a minimum follow-up of 0.50 years and a maximum of 13.33 years.

All BHVs in the collection were examined using clinical multislice computed tomography (MSCT), which provides adequate visualization of calcific deposits, on a LightSpeed™ VCT 64 scanner (General Electric, USA). During scanning, the samples were placed on a flat surface with the commissural pillars facing upward. The CT acquisition parameters were as follows: tube voltage 120 kV, tube current 160 mA, gantry rotation time 0.9 s, scan duration 6.8 s, and table speed 39.37 mm/revolution. Image reconstruction was performed with a slice thickness of 0.625 mm using a standard reconstruction kernel. Maximum intensity projection (MIP) images were generated from the MSCT images of the BHVs. After that, the three leaflets were manually extracted from each such image of the prosthesis and oriented in a single position for further clustering (Fig. 1). As a result, a total of 33 valve leaflets (N = 33) were included in the analysis.

Subsequently, the resulting set of slices was analyzed in two consecutive stages: identification of typical calcification patterns through clustering, followed by numerical modeling of the stress–strain state based on the characteristics of the identified clusters.

Calcification clusters

The extracted valve leaflets were clustered according to the number of pixels corresponding to calcified regions. In accordance with published data, areas of pathological mineralization were defined as having an X-ray density of 130 Hounsfield units (HU) [16, 17] for images in 8 bits of gray scale (0–255 gray intensity). After quantifying the number of calcified pixels for all 33 leaflets, the median and quartile values for the sample were calculated. On the basis of these indicators, three distinct image groups were identified.

Numerical modeling

After obtaining the cluster data, biomechanical analysis was performed using FEM in the Abaqus engineering analysis environment (Dassault Systèmes, France) with an explicit solver. The 3D computational model of the bioprosthetic valve comprised three leaflets and a two-component supporting frame, incorporating polypropylene and nickel–titanium elements. The material properties of all prosthetic components were defined based on manufacturer-provided specifications [18] and literature sources [19, 20]. All components were assembled into a single model using a pairing approach, as previously described in our earlier work [21]. Boundary conditions applied to the valve apparatus corresponded to normotensive pressure [22] at a heart rate of 70 beats per minute (Fig. 2).

The resulting 3D model was subsequently modified in accordance with the clustering results obtained in Stage I of the study. To do this, images of the calcium areas of each cluster were superimposed on the prosthesis leaflets, assigning the corresponding properties to the elements of the calculation grid based on data from the

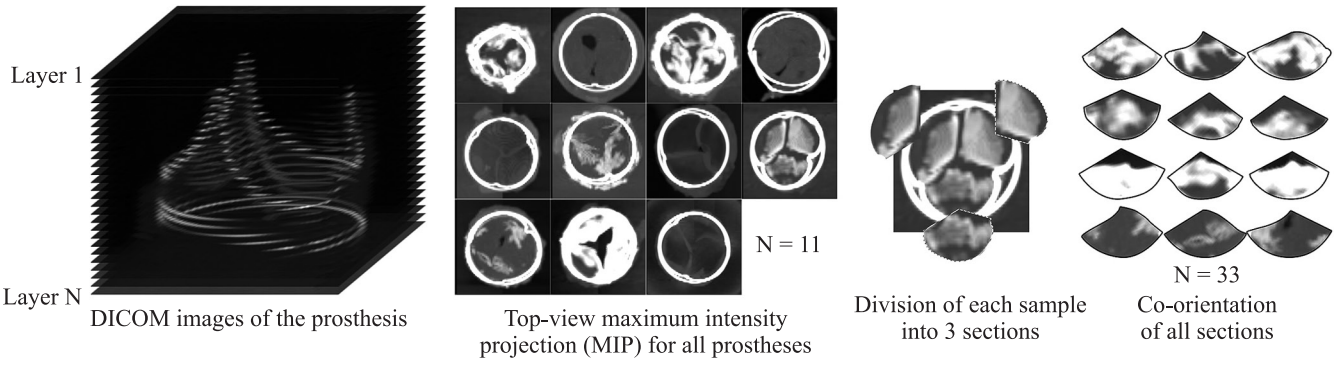

Fig. 1. DICOM image processing design for calcification intensity clustering

literature [19]. The unchanged material (non-calcified) was modeled as bovine xenopericardial tissue stabilized with ethylene glycol diglycidyl ether, as used in the manufacture of prostheses. The mechanical properties of this material and their application for FEM modeling have been described previously in our work based on experimental data [23]. Leaflet–leaflet interactions were defined using a linear soft contact formulation ("linear pressure–overclosure") with a normal stiffness of 0.2 and Coulomb friction in the tangential direction with a friction coefficient of 0.2. The numerical analysis focused on maximum principal stress (S) and material strain (LE).

Statistical analysis

Descriptive statistical methods were applied. Quantitative data were presented as the mean ± standard deviation or as the median with the 25th and 75th percentiles, as well as minimum and maximum values, where appropriate. All statistical calculations were performed using built-in functions of the NumPy library (version 1.24.4) in the Python programming environment (version 3.9).

RESULTS

Calcification clusters

During clustering, three clusters were identified (Fig. 3a): no calcification, defined as images with a pixel count below or equal to the median (≤6 pixels); mild calcification, characterized by pixel counts between the median and the third quartile (6–473 pixels); and severe calcification, defined as pixel counts equal to or exceeding the third quartile (≥473 pixels). The resulting calcium distribution patterns were conditionally labeled as clusters 0, 1, and 2, respectively. For numerical modeling, valve regions corresponding to mild and severe mineralization (clusters 1 and 2) were classified as calcified, which corresponded to probability values exceeding 50% (Fig. 3b).

To assess clustering quality, the silhouette was calculated [24], and yielded a value of 0.44, indicating moderate yet acceptable separability among the three identified groups (no calcification, mild calcification, and severe calcification).

Numerical modeling

The clusters obtained in the previous stage were subsequently mapped onto the mitral valve prosthesis model. Each such model was labeled using a triplet notation that reflects the cluster assignment for each of the three valve leaflets (Fig. 4a). This approach yielded ten unique calcification patterns: 0-0-0, 0-0-1, 0-0-2, 0-1-1, 0-1-2, 0-2-2, 1-1-1, 1-1-2, 1-2-2, and 2-2-2. In this notation, 0 denotes a leaflet without calcification, 1 corresponds to the mild calcification cluster, and 2 represents the severe calcification cluster (Fig. 4b).

The intact BHV, in which all three leaflets were free of calcification (configuration 0-0-0), was used as the initial state (Fig. 5).

Numerical modeling revealed localized peak values of maximum principal stress (S = 2.884 MPa) and material strain (LE = 0.385 mm/mm), concentrated in the commissural strut region at the leaflet attachment edge. In contrast, stress and strain within the leaflet dome were substantially lower, not exceeding S = 0.500 MPa and LE = 0.160 mm/mm. Torsional deformation of the valve apparatus was observed in the central region, demonstrating qualitative agreement with data from full-scale

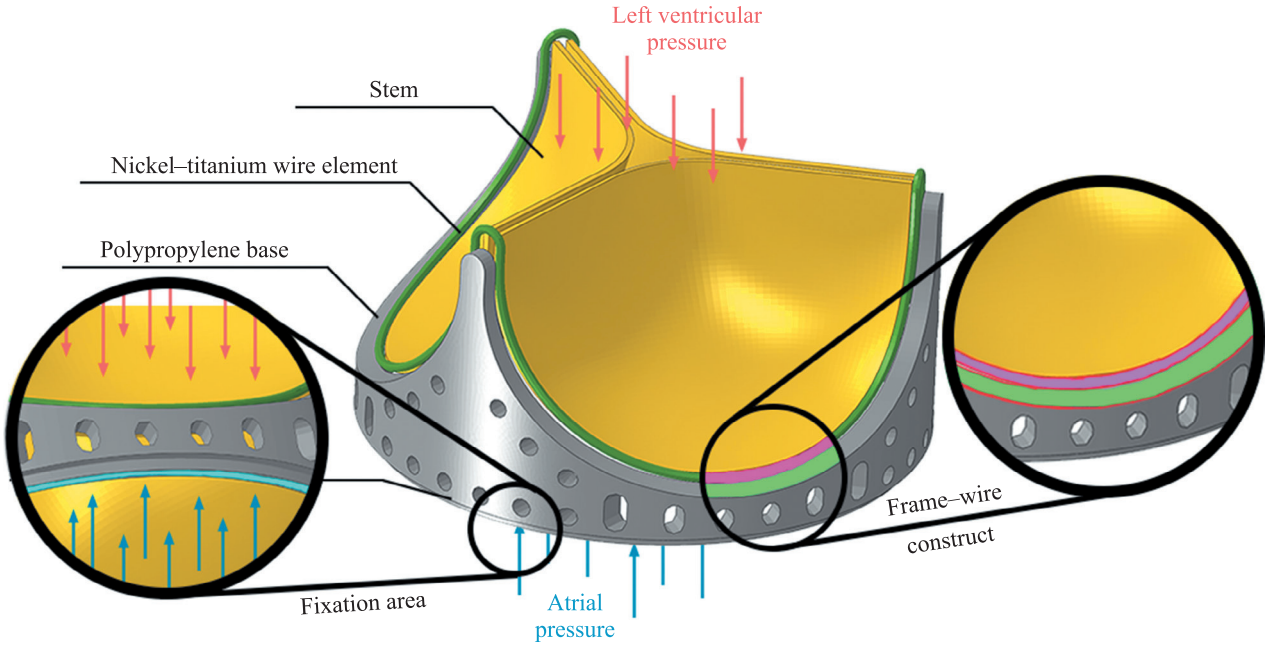

Fig. 2. Visualization of the numerical computation model with indicated boundary condition regions

experimental studies of similar aortic-position prostheses [25]. Subsequent addition of calcification clusters to the model can be interpreted as progressive valve stenosis, ranging from minor focal inclusions (0-0-1) to extensive leaflet damage (2-2-2). The results are shown in Fig. 6.

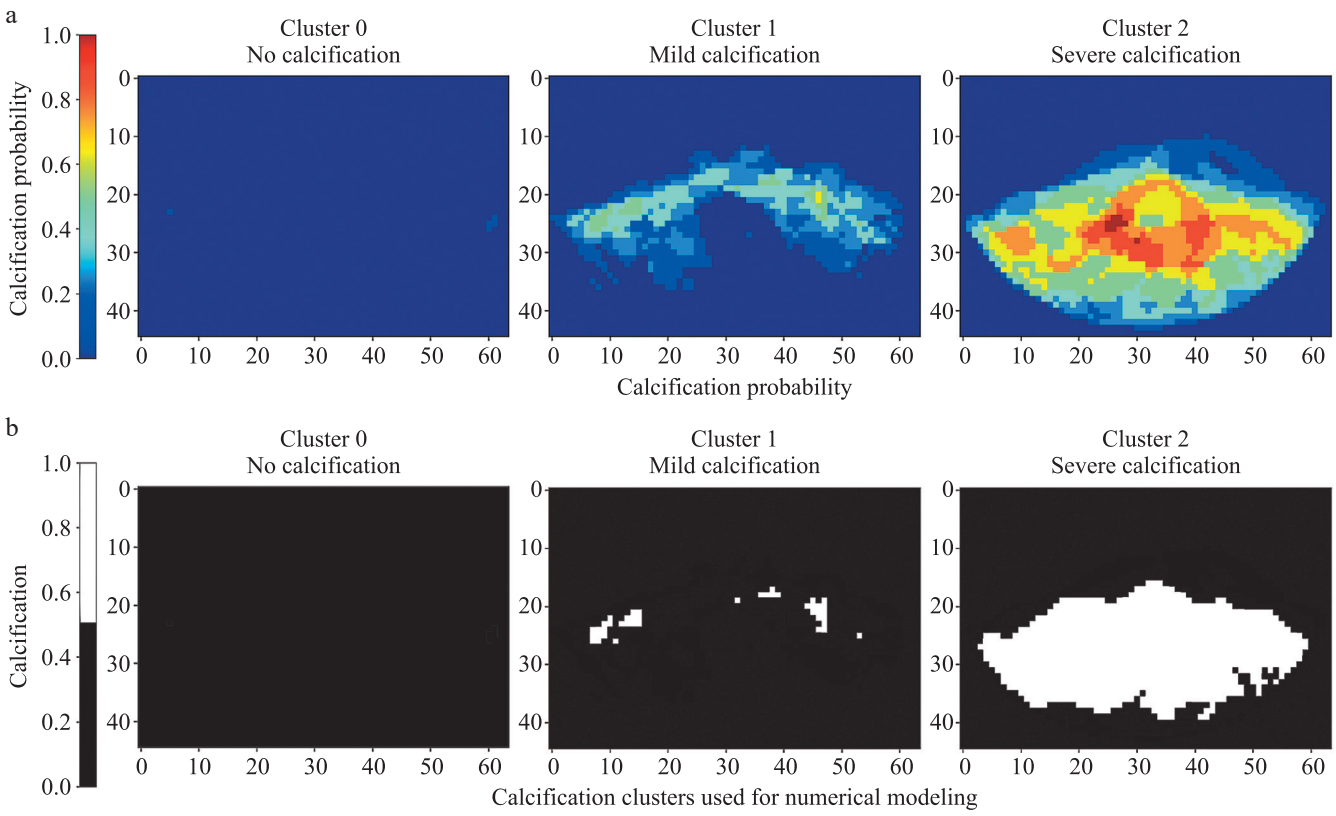

Fig. 3. Results of explanted prosthetic valve processing. a: Calcification clusters obtained; b: Clusters with calcification probability of [0.5–1] (fractions)

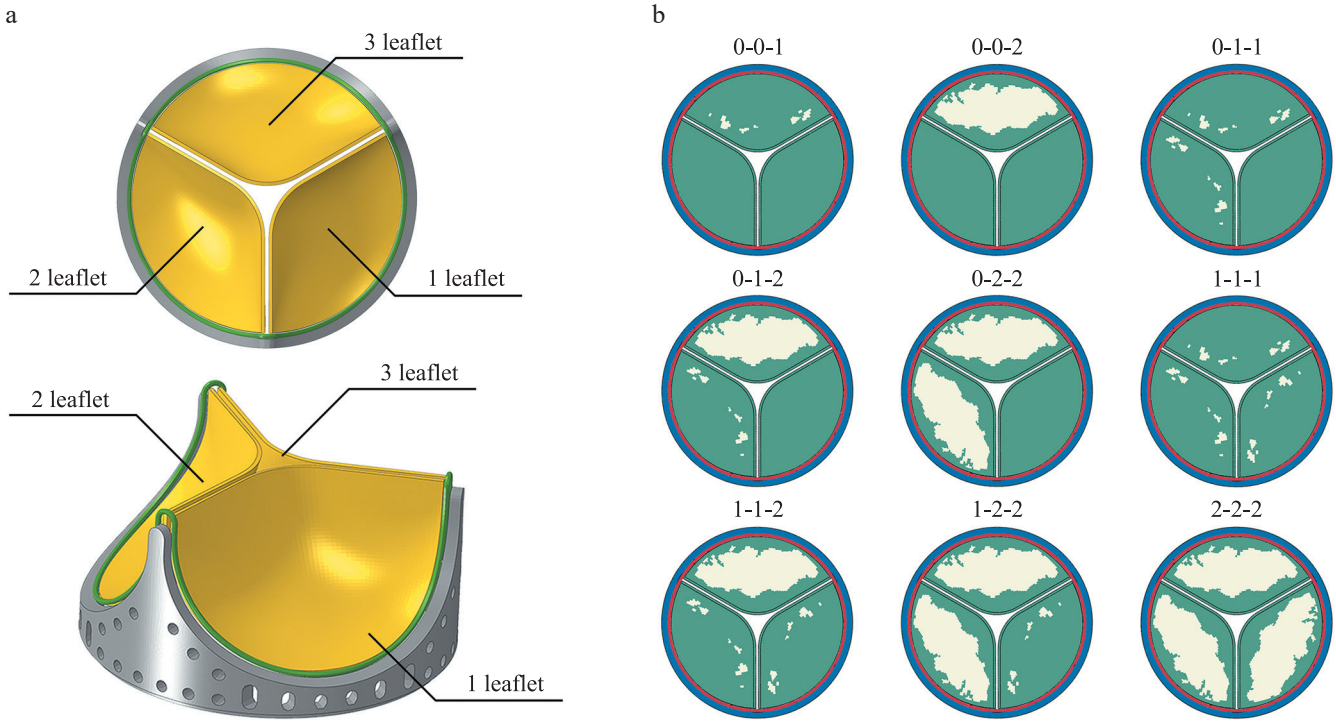

Fig. 4. Principle of forming the triplet number: (a) serial numbering of valve leaflet models; (b) superposition of calcification clusters onto the leaflet model

Numerical analysis of the prosthetic valve models (Fig. 6a–b) showed that inclusion of the second calcification cluster (triplets 0-0-2, 0-1-2, 0-2-2, 1-1-2, 1-2-2, and 2-2-2) led to the emergence of regions with elevated stress and strain in the suture edge zone – features absent in the intact case. In these models, maximum principal stress increased to S = 2.035–2.812 MPa (+283–391%), while ma-

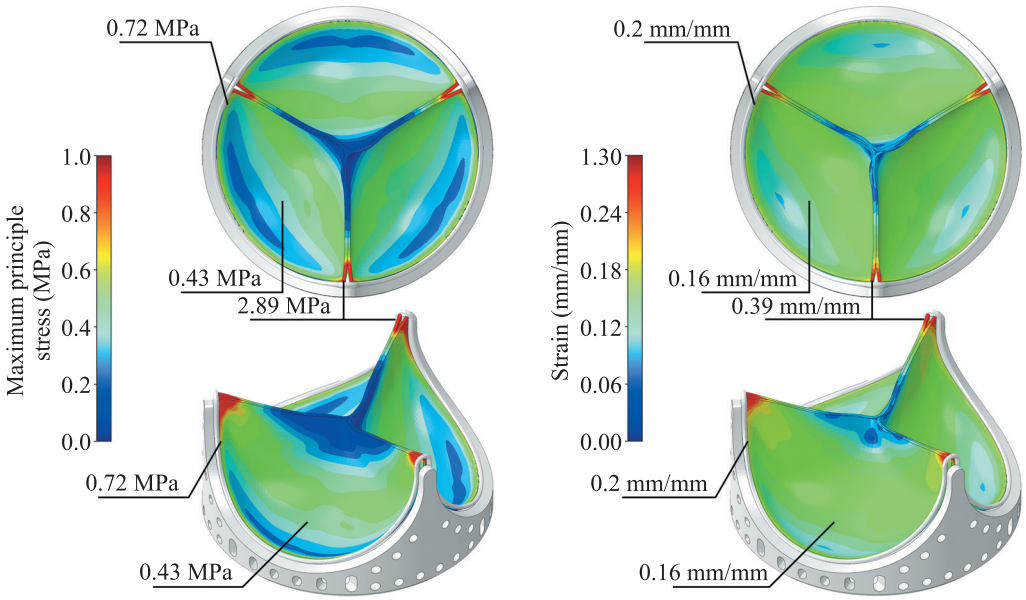

Fig. 5. Results of numerical simulation performed for the intact prosthesis

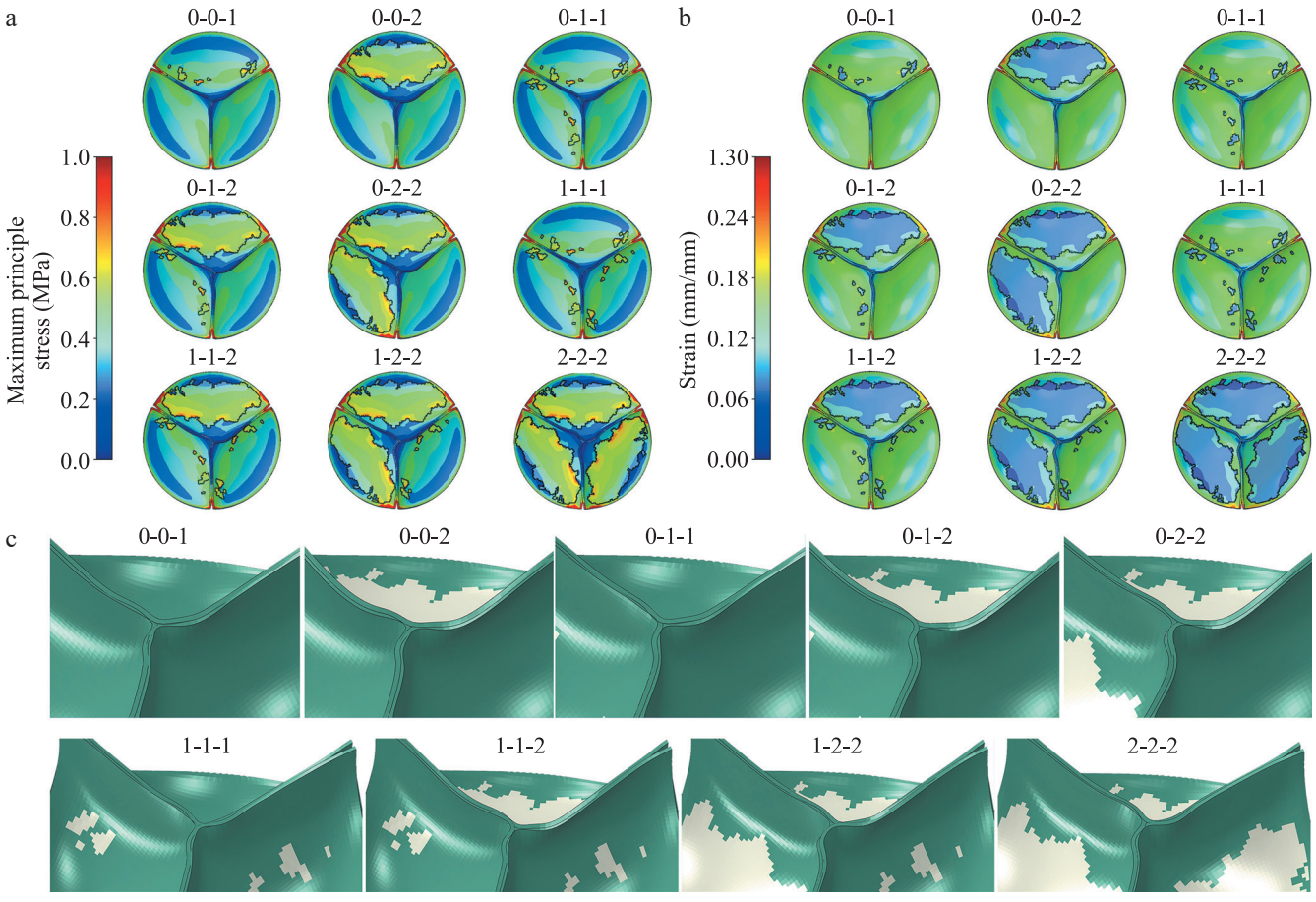

Fig. 6. Results of numerical modeling of calcium deposit clusters. Top-view contour plots show (a) maximum principal stress (MPa) and (b) strain (mm/mm). The contours of calcium clusters are outlined in black. (c) Enlarged isometric views of the valve closure region, where green indicates the bioprosthetic material and white denotes mineralized areas

terial strain rose to LE = 0.327–0.384 mm/mm (+161–189%).

The addition of the first cluster (triplets 0-0-1, 0-1-1, 0-1-2, 1-1-1, 1-1-2, and 1-2-2) did not have such an effect.

There are distinct local increases in peak stresses in the mineralization zones for the first cluster (triplets 0-0-1, 0-1-1, 0-1-2, 1-1-1, 1-1-2, 1-2-2) S = 1.175 MPa (+276%) and the second cluster S = 1.193 MPa (+280%) compared to the intact model in a similar zone (S = 0.426 MPa). In addition, a decrease in maximum strain LE = 0.108–0.117 mm/mm (a drop of 32%–26%) was noted for both clusters.

Qualitative analysis of valve closure revealed changes in the distribution of both maximum principal stress and strain fields. In cases where only the first or second cluster is present in the model on the third leaflet (Fig. 6c: 0-0-1 and 0-0-2; see Table 4), a reduction in the mean strain values (LE = 0.132 ± 0.039 mm/mm and LE = 0.120 ± 0.046 mm/mm, respectively) compared with the intact model (LE = 0.134 ± 0.037 mm/mm) resulted in leaflet "overlap" during coaptation. A similar behavior was observed in configurations with one unaffected leaflet (Fig. 6c: 0-1-1 and 0-2-2). Model 0-1-2 is distinctive in that it includes all three cluster variants. The second and third leaflets exhibited a smooth, untwisted coaptation, whereas the first (intact) leaflet showed the greatest degree of bending. This finding indicates that the presence of calcification on even a single leaflet (clusters 1 or 2) alters the mechanical behavior of the entire valve apparatus, leading to overlap or excessive bending of non-calcified (cluster 0) leaflets within the coaptation zone. In contrast, when all three leaflets were affected by calcification (Fig. 6c: 1-1-1, 1-1-2, 1-2-2, and 2-2-2), the prosthesis demonstrated a symmetrical closure pattern, with no single leaflet overlapping the others.

The next stage of the study evaluated the effect of progressive calcification – defined as an increase in the total proportion of rigid inclusions up to 42% of the leaflet volume in configuration 2-2-2 – on the peak and mean values of maximum principal stress and strain. The results are shown in Fig. 7.

The image shown (Fig. 7) demonstrates that increasing the degree of mitral valve calcification leads to two interrelated effects. First, the peak values of maximum principal stress showed a clear monotonic decrease (Fig. 7a; Tables 3, 5): from S = 2.884 MPa in the intact valve (Fig. 5, configuration 0-0-0) to S = 2.774 MPa (–3.8%) in the model with one calcification cluster on each leaflet (Fig. 6a, 1-1-1; Table 5), and further to S = 2.117 MPa (–26.6%) in the fully calcified configuration (Fig. 6a, 2-2-2; Table 5). A similar trend was observed for strain (Fig. 7b; Tables 4, 6): peak strain decreased from LE = 0.384 mm/mm in the intact model to LE = 0.378 mm/mm (–1.6%) for configuration 1-1-1, and to LE = 0.333 mm/mm (–13.3%) for configuration 2-2-2. Notably, in all cases, these peak values were loca-

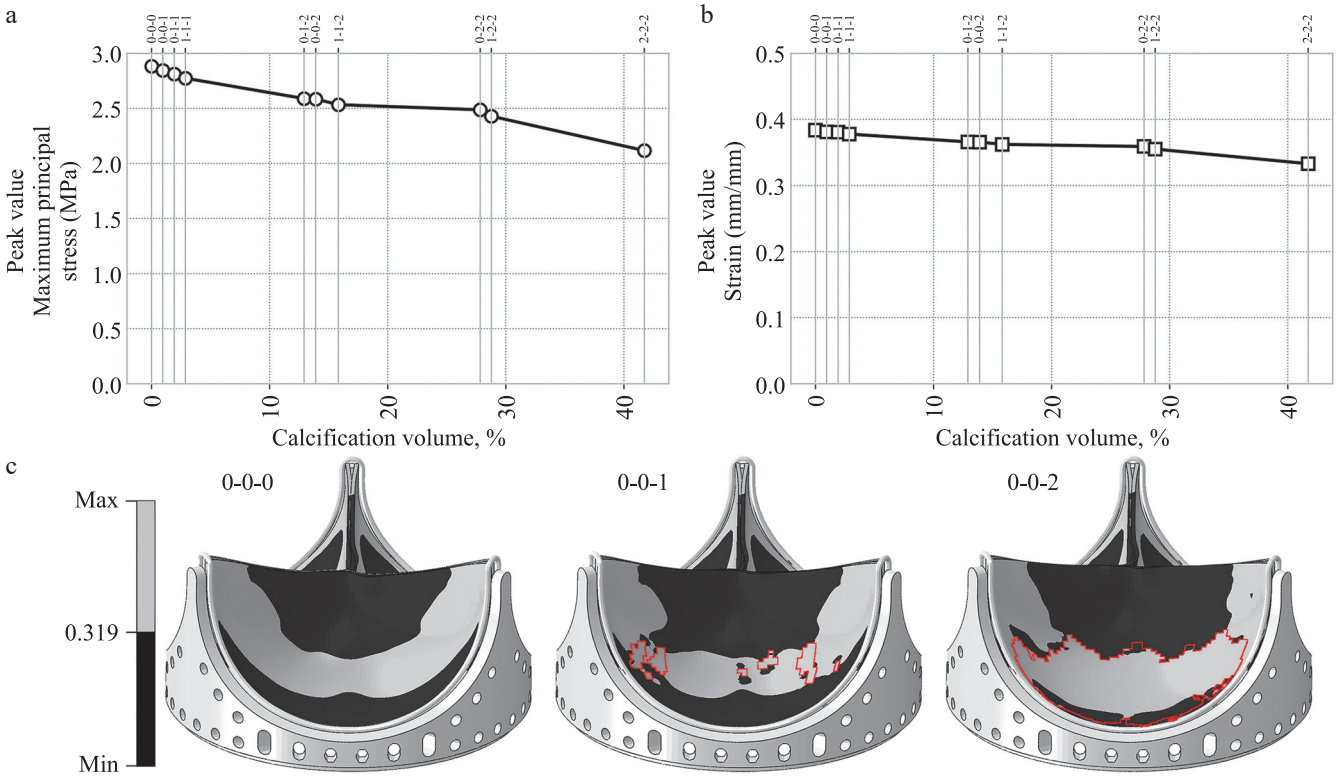

Fig. 7. Assessment of changes in peak values. (a) Maximum principal stress (MPa, S). (b) Strain (mm/mm, LE). (C) Binary map of zones with increased risk of calcification, with calcification cluster boundaries highlighted in red

lized in the region of the commissural pillars along the suture edge (Fig. 6a).

When assessing the differences in the stress-strain state, cluster 1 consistently exhibited higher mean values of both maximum principal stress (Table 5; S = 0.621 MPa) and strain (Table 6; LE = 0.060 mm/mm) than cluster 2 (S = 0.514 MPa and LE = 0.050 mm/mm, respectively). Overall, increasing calcification volume was associated with a rise in the mean values and standard deviations of both maximum principal stress (Table 3) and strain (Table 4), with average stress increasing from S = 0.319 MPa in the intact prosthesis to S = 0.360 MPa in the case of complete leaflet mineralization.

Secondly, spatial localization of calcification influenced the adjacent, non-calcified leaflets (Table 1; triplets 0-0-1, 0-0-2, 0-1-1, 0-1-2, and 0-2-2). Compared with the intact model, these configurations demonstrated a general tendency toward reduced peak maximum principal stress values (by up to 22.3% from S = 2.884 MPa) as well as a decrease in mean stress across the leaflet (by approximately 5% from S = 0.319 MPa). Average stress levels across the entire leaf in the presence of only one cluster (Table 1, triplets 0-0-1 and 0-1-1) increased slightly by 0.6–0.9%, and in the presence of only the second (0-0-2 and 0-2-2) – decreased by 2.2–5%. When both cluster types were co-localized, a comparable decrease in mean stress was observed (–1.9%; Table 1, configuration 0-1-2).

When strain was analyzed, the intact model showed peak and mean strain values of LE = 0.384 mm/mm and LE = 0.134 mm/mm, respectively. Overall, the presence of calcification was associated with reduced peak leaflet strain (Fig. 7b; Table 2, Table 6). Cluster 1 had a negligible effect on leaflet stiffness, with peak strain decreasing by only 0.8% and 3.9% in triplets 0-0-1 and 0-1-1, respectively.

Table 1

Changes in maximum principal stress (S) in leaflets of Cluster 0 compared with the intact model

Model no.	Peak value, MPa (+/–% change)	Average value, MPa (+/–% change)
0-0-0	2.884	0.319
0-0-1	2.845 (–1.4%)	0.321 (+0.6%)
0-0-2	2.570 (–10.9%)	0.312 (–2.2%)
0-1-1	2.632 (–8.7%)	0.322 (+0.9%)
0-1-2	2.536 (–12.1%)	0.313 (–1.9%)
0-2-2	2.242 (–22.3%)	0.303 (–5.0%)

Table 2

Changes in maximum principal stress (S) in leaflets of Cluster 0 compared with the intact model

Model no.	Peak value (mm/mm) (+/–% change)	Average value (mm/mm) (+/–% change)
0-0-0	0.384	0.134
0-0-1	0.381 (–0.8%)	0.134 (0%)
0-0-2	0.365 (–5.0%)	0.132 (–1.5%)
0-1-1	0.369 (–3.9%)	0.134 (0%)
0-1-2	0.363 (–5.5%)	0.132 (–1.5%)
0-2-2	0.342 (–10.9%)	0.130 (–3.0%)

Table 3

Statistical analysis of the maximum principal stress (MPa, S) for the model as a whole. Negative values indicate compressive stress

Model	Avg.	Standard deviation	Min	Q25%	Q50%	Q75%	Max
0-0-0	0.319	0.178	–0.123	0.193	0.325	0.439	2.884
0-0-1	0.321	0.194	–0.131	0.191	0.318	0.442	2.845
0-0-2	0.335	0.202	–0.136	0.191	0.334	0.455	2.585
0-1-1	0.322	0.197	–0.133	0.189	0.312	0.444	2.812
0-1-2	0.332	0.198	–0.136	0.189	0.325	0.455	2.590
0-2-2	0.348	0.213	–0.138	0.185	0.344	0.482	2.487
1-1-1	0.322	0.200	–0.137	0.187	0.306	0.446	2.774
1-1-2	0.335	0.208	–0.140	0.186	0.320	0.469	2.534
1-2-2	0.348	0.216	–0.142	0.182	0.336	0.490	2.429
2-2-2	0.360	0.223	–0.142	0.176	0.361	0.524	2.117

Table 4

Statistical analysis of strain (mm/mm, LE) for the model as a whole

Model	Avg.	Standard deviation	Min	Q25%	Q50%	Q75%	Max
0-0-0	0.134	0.037	0.004	0.105	0.141	0.162	0.385
0-0-1	0.132	0.039	0.007	0.103	0.138	0.163	0.381
0-0-2	0.120	0.046	0.007	0.086	0.126	0.158	0.366
0-1-1	0.131	0.040	0.003	0.101	0.136	0.162	0.381
0-1-2	0.121	0.045	0.007	0.089	0.126	0.157	0.366
0-2-2	0.106	0.050	0.007	0.059	0.107	0.149	0.359
1-1-1	0.130	0.041	0.005	0.099	0.133	0.162	0.378
1-1-2	0.117	0.047	0.007	0.082	0.121	0.155	0.362
1-2-2	0.105	0.050	0.007	0.059	0.104	0.146	0.355
2-2-2	0.093	0.050	0.008	0.051	0.079	0.134	0.333

Table 5

Statistical analysis of maximum principal stress (MPa, S) stratified by clusters. Negative values indicate compressive stress

Model	Cluster number	Avg.	Standard deviation	Min	Q25%	Q50%	Q75%	Max
0-0-0	0	0.319	0.178	–0.123	0.193	0.325	0.439	2.884
0-0-1	0	0.321	0.190	–0.131	0.193	0.326	0.441	2.845
	1	0.322	0.201	–0.130	0.188	0.305	0.445	2.807
0-0-2	0	0.312	0.182	–0.136	0.190	0.317	0.431	2.570
	2	0.380	0.231	–0.136	0.193	0.381	0.541	2.585
0-1-1	0	0.321	0.190	–0.130	0.192	0.326	0.443	2.632
	1	0.322	0.200	–0.133	0.187	0.306	0.446	2.812
0-1-2	0	0.313	0.173	–0.136	0.190	0.318	0.434	2.536
	1	0.311	0.189	–0.131	0.183	0.295	0.429	2.422
	2	0.380	0.232	–0.136	0.193	0.383	0.543	2.590
0-2-2	0	0.303	0.173	–0.137	0.186	0.308	0.419	2.242
	2	0.370	0.227	–0.138	0.185	0.372	0.534	2.487
1-1-1	1	0.322	0.200	–0.137	0.187	0.306	0.446	2.774
1-1-2	1	0.314	0.192	–0.140	0.183	0.298	0.433	2.486
	2	0.379	0.231	–0.136	0.192	0.381	0.542	2.534
1-2-2	1	0.301	0.180	–0.142	0.180	0.286	0.413	2.166
	2	0.371	0.228	–0.138	0.185	0.372	0.535	2.429
2-2-2	2	0.360	0.223	–0.142	0.176	0.361	0.524	2.117

Table 6

Statistical analysis of strain (mm/mm, LE) stratified by clusters

Model	Cluster number	Avg.	Standard deviation	Min	Q25%	Q50%	Q75%	Max
0-0-0	0	0.134	0.037	0.004	0.105	0.141	0.162	0.384
0-0-1	0	0.134	0.039	0.007	0.104	0.140	0.163	0.381
	1	0.130	0.041	0.014	0.100	0.134	0.161	0.381
0-0-2	0	0.132	0.038	0.014	0.103	0.138	0.161	0.365
	2	0.097	0.052	0.007	0.053	0.084	0.139	0.366
0-1-1	0	0.134	0.039	0.012	0.104	0.141	0.163	0.369
	1	0.130	0.041	0.003	0.099	0.134	0.161	0.381
0-1-2	0	0.132	0.037	0.015	0.104	0.138	0.161	0.363
	1	0.127	0.039	0.025	0.097	0.130	0.158	0.354
	2	0.097	0.052	0.007	0.053	0.084	0.140	0.366
0-2-2	0	0.130	0.037	0.029	0.101	0.136	0.158	0.342
	2	0.095	0.051	0.007	0.052	0.082	0.137	0.359
1-1-1	1	0.130	0.041	0.005	0.099	0.133	0.162	0.378
1-1-2	1	0.128	0.040	0.007	0.098	0.131	0.159	0.360
	2	0.097	0.052	0.007	0.053	0.084	0.139	0.362
1-2-2	1	0.125	0.038	0.025	0.097	0.127	0.156	0.337
	2	0.095	0.051	0.007	0.052	0.081	0.137	0.355

In contrast, cluster 2 produced a moderate stiffening effect: peak strain decreased by 5.0% and 10.9%. The co-localization of both cluster types resulted in a comparable reduction in peak strain (5.5%), similar to that observed for triplets 0-0-2. In terms of average values, cluster 1 did not cause any changes, while cluster 2 (triplets 0-0-2 and 0-2-2) and the combination (triplet 0-1-2) reduced them by 1.5% for all except 0-2-2 (–3.0%).

A qualitative analysis of the stress–strain state maps showed that, in the intact prosthesis, a distinct zone of elevated stresses was present along the leaflet dome, with maximum principal stress values ranging from S = 0.44 to 0.48 MPa, exceeding the mean stress level of the entire model (S = 0.319 MPa) (Fig. 7b). Notably, this region coincided with cluster 1 location, which in the present study was conditionally interpreted as representing an early stage of calcification. The stress level in this dome region was approximately 40–50% higher than the average stress value across the entire leaflet of the intact model (S = 0.319 MPa, see Table 3).

DISCUSSION

Numerical modeling results for the intact variant revealed a stress distribution pattern known for BHVs [26, 27]. The maximum principal stress (S = 2.885 MPa) and strain (LE = 0.385 mm/mm) were observed in the commissural pillar zone, whereas lower values were detected in the leaflet dome (S = 0.450 MPa and LE = 0.145 mm/mm, respectively). Similar findings have been reported by Nestola et al. [28] who investigated incompressible fluid flow through an aortic BHV using a fluid–structure interaction (FSI) approach. Their results demonstrated that peak stresses are concentrated near the leaflet attachment zones and commissures, which is consistent with the areas of peak mechanical stress identified in our FEM model. Thus, despite methodological differences between FEM and FSI simulations, both approaches indicate that the commissural pillar region represents a critical zone of stress concentration. The elevated stress levels observed in these areas (up to 2.885 MPa) are primarily associated with tensile loading of the valve material during closure and are in good quantitative agreement with previously published data, reporting peak stress values in the range of 2.087–2.500 MPa [29–31].

The sequential inclusion of calcification clusters in the model demonstrated that progressive mineralization, associated with an increase in the volume fraction of mineral inclusions up to 42%, led to a gradual stiffening of the valve leaflets and a corresponding reduction in their strain (strain decreased by approximately 11% when comparing the intact model [0-0-0] with the fully calcified configuration (2-2-2), with LE declining from 0.384 to 0.333 mm/mm (–13.3%). This effect could potentially lead to an increase in afterload on the myocardium and elevate the risk of left ventricular hypertrophy during long-term use of prostheses affected by SVD [32, 33]. Previous studies have linked reduced leaflet mobility and valve stenosis to increases in the mean diastolic pressure gradient and changes in intracardiac hemodynamics. These findings are further supported by published data demonstrating that rigid inclusions within the mitral valve increase local hydrodynamic stresses, thereby promoting regurgitation and flow turbulence [34].

This study revealed differences in the distribution of mechanical stresses within the prosthesis in the presence of calcium deposits of varying severity. These findings are consistent with the results reported by Qin et al. [14], who showed, using an aortic valve model, that localized mechanical stress gradients in BHVs may act as initiators of subsequent calcification, thereby creating a self-reinforcing cycle of material degradation. FEM-based investigations of calcified valve leaflets similarly indicate that mechanical stress is a critical factor in both the initiation and spread of calcification [14, 35]. In particular, the work of Arzani et al. [15], which focused on modeling the function of the native aortic valve, demonstrated that calcium accumulation can originate and progress in areas subjected to increased circumferential strain. This observation closely aligns with our results, in which maximum principal stresses were concentrated at the boundaries of calcium deposits, in the suture margin area.

In addition, the results showed that although calcification reduced peak mechanical loads within the leaflet tissue, it simultaneously changed the valve closure pattern in the central zone, leading to overlapping of calcified leaflets onto relatively intact ones. This phenomenon may be associated with increased risk of accelerated wear at the free edge of the BHV [3, 36]. According to reports [3, 37], such alterations contribute to regurgitation, increased transvalvular pressure gradients, elevated hydraulic resistance, and reduced effective volumetric output of the prosthesis. Experimental studies [20, 30, 31, 38, 39] support these observations and emphasize the importance of accounting for both mechanical and hemodynamic factors when evaluating the durability and functional performance of BHVs.

Identification of regions where maximum principal stresses exceeded the average values in the intact model (Fig. 7b) revealed a clear spatial overlap between stress levels of 0.44–0.48 MPa (1.4–1.5 times higher than the mean value of S = 0.319 MPa) and areas corresponding to early-stage calcification. Comparable findings were reported by Qin et al. [14], who demonstrated that localized stress concentrations in aortic valve leaflets correlate with both the direction and rate of mineralization growth and are closely related to average stress levels. The model proposed by Arzani et al. [15] showed that rigid inclusions generate zones of reduced strain, which in turn promote further progression of mineralization and establish a self-sustaining cycle of calcification. This effect was attributed to localized stiffness gradients at the boundaries of mineralized regions, leading to stress

redistribution and strain amplification in adjacent tissues. Notably, mitral valve prostheses undergo higher mechanical stress compared with other valve positions, primarily due to hemodynamic characteristics [40].

In summary, the following conclusions can be drawn from the results:

1. Calcification of the mitral BHV is closely related to the stress–strain state of the valve: lower average values of maximum principal stress are associated with a reduced likelihood of mineralization developing in the leaflet dome.
2. Areas where the maximum principal stress exceeds the average by 40–50% correspond to the locations of calcification clusters;

CONCLUSION

The study conducted on 33 explanted BHVs showed that calcification patterns significantly influence the biomechanical behavior of bioprosthetic mitral valves. Three distinct mineralization patterns were identified: no calcification (cluster 0), mild calcification (cluster 1), and severe calcification (cluster 2). FEM analysis revealed a spatial correlation between regions of maximum principal stress exceeding S >0.319 MPa in the intact model and the locations of calcification clusters, with these areas exhibiting a 40–50% higher local stress in the valve leaflet dome. Importantly, the introduction of clusters 1 and 2 into the valve leaflet did not alter the localization of these high-stress regions. FEM results indicated that the presence of at least one cluster 0 or 1 did not significantly influence mean maximum principal stress (decrease ≤5%) or mean strain (decrease ≤3%).

This work was carried out as part of the fundamental research program of the Research Institute for Complex Issues of Cardiovascular Diseases on the topic: "Molecular, cellular, and biomechanical mechanisms of cardiovascular disease pathogenesis in the development of new treatment methods for cardiovascular diseases based on personalized pharmacotherapy, minimally invasive medical devices, biomaterials, and tissue-engineered implants", topic code 0419-2022-0001.

The authors declare no conflict of interest.

REFERENCES

1. *Bokeriya LA, Milievskaya EB, Pryanishnikov VV, Yurlov IA*. Serdechno-sosudistaya khirurgiya – 2022. Bolezni i vrozhdennye anomalii sistemy krovoobrashcheniya. M.: NMITS SSKh im. A.N. Bakuleva, 2023; 343.
2. *Alekyan BG, Grigor'yan AM, Staferov AV, Karapetyan NG*. Endovascular diagnostics and treatment in the Russian Federation (2021). *Russian Journal of Endovascular Surgery*. 2022; 9 (S): 1–254. doi: 10.24183/2409-4080-2022-9S.
3. *Kostyunin AE, Yuzhalin AE, Rezvova MA, Ovcharenko EA, Glushkova TV, Kutikhin AG*. Degeneration of bioprosthetic heart valves: Update 2020. *J Am Heart Assoc*. 2020; 9 (19): e018506. doi: 10.1161/JAHA.120.018506.
4. *Kudryavtseva YuA, Nasonova MV, Akentieva TN, Burago AYu, Zhuravlyova IYu*. The role of suture material in the calcification of cardiovascular bioprosthesis. *Complex Issues of Cardiovascular Diseases*. 2013; (4): 22–27. [In Russ, English abstract]. doi: 10.17802/2306-1278-2013-4-22-27.
5. *Kostyunin AE, Glushkova TV, Klyshnikov KY, Rezvova MA, Akentyeva TN, Onishchenko PS, Ovcharenko EA*. Impact of cyclic loading on the resistance of epoxy-treated bovine pericardium modified with polyvinyl alcohol to calcification and proteolytic degradation. *Complex Issues of Cardiovascular Diseases*. 2024; 13 (3): 54–62. doi: 10.17802/2306-1278-2024-13-3-54-62.
6. *Rodriguez-Gabella T, Voisine P, Puri R, Pibarot P, Rodés-Cabau J*. Aortic Bioprosthetic Valve Durability: Incidence, Mechanisms, Predictors, and Management of Surgical and Transcatheter Valve Degeneration. *J Am Coll Cardiol*. 2017; 70 (8): 1013–1028. doi: 10.1016/j.jacc.2017.07.715.
7. *Senage T, Paul A, Le Tourneau T, Fellah-Hebia I, Vadori M, Bashir S et al*. The role of antibody responses against glycans in bioprosthetic heart valve calcification and deterioration. *Nat Med*. 2022; 28 (2): 283–294. doi: 10.1038/s41591-022-01682-w.
8. *Wen S, Zhou Y, Yim WY, Wang S, Xu L, Shi J et al*. Mechanisms and Drug Therapies of Bioprosthetic Heart Valve Calcification. *Front Pharmacol*. 2022; 13: 909801. doi: 10.3389/fphar.2022.909801.
9. *Sinusas AJ*. Evaluation of Bioprosthetic Valve Deterioration: Is Tissue Analysis Sufficient? *JACC Basic Transl Sci*. 2023; 8 (7): 881–883. doi: 10.1016/j.jacbts.2023.03.023.
10. *Hamid MS, Sabbah HN, Stein PD*. Vibrational analysis of bioprosthetic heart valve leaflets using numerical models: Effects of leaflet stiffening, calcification, and perforation. *Circ Res*. 1987; 61 (5): 687–694. doi: 10.1161/01.RES.61.5.687.
11. *Claiborne TE, Sheriff J, Kuetting M, Steinseifer U, Slepian MJ, Bluestein D*. *In vitro* evaluation of a novel hemodynamically optimized trileaflet polymeric prosthetic heart valve. *J Biomech Eng*. 2013; 135 (2): 021021. doi: 10.1115/1.4023235.
12. *Claiborne TE, Xenos M, Sheriff J, Chiu WC, Soares J, Alemu Y et al*. Toward optimization of a novel trileaflet polymeric prosthetic heart valve via device thrombogenicity emulation. *ASAIO J*. 2013; 59 (3): 275–283. doi: 10.1097/MAT.0b013e31828e4d80.
13. *Xuan Y, Dvir D, Wang Z, Mizoguchi T, Ye J, Guccione JM et al*. Stent and leaflet stresses in 26-mm, third-generation, balloon-expandable transcatheter aortic valve. *J Thorac Cardiovasc Surg*. 2019; 157 (2): 528–536. doi: 10.1016/j.jtcvs.2018.04.115.
14. *Qin T, Caballero A, Mao W, Barrett B, Kamioka N, Lerakis S, Sun W*. The role of stress concentration in calcified bicuspid aortic valve. *J R Soc Interface*. 2020; 17 (167): 20190893. doi: 10.1098/rsif.2019.0893.
15. *Arzani A, Mofrad MRK*. A strain-based finite element model for calcification progression in aortic valves.

J Biomech. 2017; 65: 216–220. doi: 10.1016/j.jbiomech.2017.10.014.
16. *Hou K, Tsujioka K, Yang C*. Optimization of HU threshold for coronary artery calcium scans reconstructed at 0.5-mm slice thickness using iterative reconstruction. *J Appl Clin Med Phys*. 2020; 21 (2): 111–120. doi: 10.1002/acm2.12806.
17. *Czaja-Ziółkowska M, Wasilewski J, Gąsior M, Głowacki J*. An update on the coronary calcium score: a review for clinicians. *Postepy Kardiol Interwencyjnej*. 2022; 18 (3): 201–205. doi: 10.5114/aic.2022.121035.
18. ExxonMobil. ExxonMobilTM PP1014H1 Polypropylene Homopolymer. Datasheet. 2022. p. 2. Available from: https://exxonmobilchemical.ulprospector.com/datasheet.aspx.
19. *Finotello A, Gorla R, Brambilla N, Bedogni F, Auricchio F, Morganti S*. Finite element analysis of transcatheter aortic valve implantation: Insights on the modelling of self-expandable devices. *J Mech Behav Biomed Mater*. 2021; 123: 104772. doi: 10.1016/j.jmbbm.2021.104772.
20. *Capelli C, Bosi GM, Cerri E, Nordmeyer J, Odenwald T, Bonhoeffer P et al*. Patient-specific simulations of transcatheter aortic valve stent implantation. *Med Biol Eng Comput*. 2012; 50 (2): 183–192. doi: 10.1007/S11517-012-0864-1.
21. *Onishchenko PS, Klyshnikov KYu, Ovcharenko EA* Optimization of biological heart valve prosthesis “UniLine”: new tools for improving function. *Russian Journal of Biomechanics*. 2024; 28 (1): 10–22. [In Russ, English abstract]. doi: 10.15593/RZhBiomeh/2024.1.01.
22. *Park J-H, Marwick TH*. Use and Limitations of E/e’ to Assess Left Ventricular Filling Pressure by Echocardiography. *J Cardiovasc Ultrasound*. 2011; 19 (4): 169–173. doi: 10.4250/jcu.2011.19.4.169.
23. *Onishchenko PS, Glushkova TV, Kostyunin AE, Rezvova MA, Akentyeva TN, Barbarash LS*. Computer models of biomaterials used for the manufacture of valve leaflets for heart valve prostheses. *Materials Science*. 2023; (7): 30–39. [In Russ, English abstract]. doi: 10.31044/1684-579X-2023-0-7-30-39.
24. *Rousseeuw PJ*. Silhouettes: A graphical aid to the interpretation and validation of cluster analysis. *Journal of Computational and Applied Mathematics*. 1987; 20: 53–65. doi: 10.1016/0377-0427(87)90125-7.
25. *Klyshnikov KY, Onischenko PS, Ovcharenko EA*. Study of Biomechanics of the Heart Valve Leaflet Apparatus Using Numerical Simulation Method. *Sovrem Tekhnologii Med*. 2022; 14 (2): 6–14. doi: 10.17691/stm2022.14.2.01.
26. *Pandya PK, Park MH, Zhu Y, Woo YJ*. Biomechanical analysis of novel leaflet geometries for bioprosthetic valves. *JTCVS Open*. 2023; 14: 77–86. doi: 10.1016/j.xjon.2023.04.007.
27. *Sacks MS, Mirnajafi A, Sun W, Schmidt P*. Bioprosthetic heart valve heterograft biomaterials: structure, mechanical behavior and computational simulation. *Expert Rev Med Devices*. 2006; 3 (6): 817–834. doi: 10.1586/17434440.3.6.817.
28. *Nestola MGC, Zulian P, Gaedke-Merzhäuser L, Krause R*. Fully coupled dynamic simulations of bioprosthetic aortic valves based on an embedded strategy for fluid–structure interaction with contact. *EP Europace*. 2021; 23 (Suppl 1): i96–i104. doi: 10.1093/europace/euaa398.
29. *Kim H, Lu J, Sacks MS, Chandran KB*. Dynamic simulation of bioprosthetic heart valves using a stress resultant shell model. *Ann Biomed Eng*. 2008; 36 (2): 262–275. doi: 10.1007/S10439-007-9409-4.
30. *Stanová V, Rieu R, Thollon L, Salaun E, Rodés-Cabau J, Côté N et al*. Leaflet Mechanical Stress in Different Designs and Generations of Transcatheter Aortic Valves: An *in Vitro* Study. *Struct Heart*. 2024; 8 (2): 100262. doi: 10.1016/j.shj.2023.100262.
31. *Stanová V, Godio Raboutet Y, Barragan P, Thollon L, Pibarot P, Rieu R*. Leaflet stress quantification of porcine vs bovine surgical bioprostheses: an *in vitro* study. *Comput Methods Biomech Biomed Engin*. 2022; 25 (1): 40–51. doi: 10.1080/10255842.2021.1928092.
32. *Elmariah S, Delaney JAC, Bluemke DA, Budoff MJ, O’Brien KD, Fuster V et al*. Associations of LV Hypertrophy With Prevalent and Incident Valve Calcification. *JACC Cardiovasc Imaging*. 2012; 5 (8): 781–788. doi: 10.1016/j.jcmg.2011.12.025.
33. *Fashanu OE, Upadhrasta S, Zhao D, Budoff MJ, Pandey A, Lima JAC, Michos ED*. Effect of Progression of Valvular Calcification on Left Ventricular Structure and Frequency of Incident Heart Failure (from the Multiethnic Study of Atherosclerosis). *Am J Cardiol*. 2020; 134: 99–107. doi: 10.1016/j.amjcard.2020.08.017.
34. *Li C, Tong Z, Yongheng W, Xiaoyu L, Hao G*. Fluid–structure interaction simulation of pathological mitral valve dynamics in a coupled mitral valve-left ventricle model. *Intelligent Medicine*. 2023; 03 (02): 104–114. doi: 10.1016/j.imed.2022.06.005.
35. *Pawade TA, Newby DE, Dweck MR*. Calcification in Aortic Stenosis. *J Am Coll Cardiol*. 2015; 66 (5): 561–577. doi: 10.1016/j.jacc.2015.05.066.
36. *Barannyk O, Fraser R, Oshkai P*. A correlation between long-term *in vitro* dynamic calcification and abnormal flow patterns past bioprosthetic heart valves. *J Biol Phys*. 2017; 43 (2): 279–296. doi: 10.1007/s10867-017-9452-9.
37. *Pibarot P, Dumesnil JG*. Prosthetic heart valves: selection of the optimal prosthesis and long-term management. *Circulation*. 2009; 119 (7): 1034–1048. doi: 10.1161/CIRCULATIONAHA.108.778886.
38. *Tsolaki E, Corso P, Zboray R, Avaro J, Appel C, Liebi M et al*. Multiscale multimodal characterization and simulation of structural alterations in failed bioprosthetic heart valves. *Acta Biomater*. 2023; 169: 138–154. doi: 10.1016/j.actbio.2023.07.044.
39. *Lee JH, Rygg AD, Kolahdouz EM, Rossi S, Retta SM, Duraiswamy N et al*. Fluid–Structure Interaction Models of Bioprosthetic Heart Valve Dynamics in an Experimental Pulse Duplicator. *Ann Biomed Eng*. 2020; 48 (5): 1475–1490. doi: 10.1007/s10439-020-02466-4.
40. *Liu W, Yang G*. Progressive calcification of bioprosthetic mitral valve observed during pregnancy resulting from *in vitro* fertilization: a case report. *BMC Cardiovasc Disord*. 2024; 24 (1): 506. doi: 10.1186/s12872-024-04180-8.

The article was submitted to the journal on 18.06.2025